



ARTICLE

Novel treatment for refractory rheumatoid arthritis with total glucosides of paeony and nobiletin codelivered in a self-nanoemulsifying drug delivery system

Biao Qu^{1,2}, Xiao-lin Wang^{1,3}, De-chong Zheng^{1,2}, Chu-tian Mai^{1,2}, Zhong-qiu Liu⁴, Hua Zhou^{1,2} and Ying Xie^{1,3}

Patients with refractory rheumatoid arthritis (RA) remain a substantial clinical problem, while the overexpression of P-glycoprotein (P-gp) on their lymphocytes may contribute to resistance to anti-rheumatic drugs. This study aims to develop a novel treatment for refractory RA consisting of the combination of total glucosides of paeony (TGP) and the P-gp inhibitor nobiletin (N), which are codelivered in a self-nanoemulsifying drug delivery system (SNEDDS). Based on the solubility, compatibility, and pseudoternary phase diagram tests, a nano-SNEDDS formulation composed of capryol 90-cremophor EL35-tcranscutol HP (CET) to codeliver TGP and N was developed, and this formulation increased the bioavailability of TGP by 435.04% (indicated with paeoniflorin). A modified adjuvant-induced arthritis (AIA) rat model was verified for the overexpression of P-gp in lymphocytes and resistance to methotrexate (MTX) treatment at the reported anti-inflammatory dosage. CET formulation not only increased the solubility and permeability of TGP but also inhibited the function and expression of P-gp, leading to enhanced bioavailability and intracellular concentration in the lymphocytes of AIA rats and consequently boosting the anti-arthritic effects of TGP. Moreover, TGP and N coloaded CET reduced the expression of P-gp in AIA rats partly by inhibiting the phosphorylated AKT and HIF-1 α pathways. In summary, TGP-N coloaded SNEDDS is a novel and effective treatment for refractory RA.

Keywords: refractory rheumatoid arthritis; P-glycoprotein; total glucosides of paeony; nobiletin; self-nanoemulsifying drug delivery systems

Acta Pharmacologica Sinica (2022) 43:2094–2108; <https://doi.org/10.1038/s41401-021-00801-6>

INTRODUCTION

Rheumatoid arthritis (RA) is a chronic systemic inflammatory disease characterized by erosive synovitis and severe joint destruction and disability [1, 2] that is accompanied with damage to multiple tissues because the immune system attacks healthy tissue [3]. Disease-modifying anti-rheumatic drugs (DMARDs) and biological DMARDs represent commonly used agents to relieve the symptoms of RA [4, 5].

However, a subgroup of patients (6%–21%), defined as “refractory” or “treatment-resistant” RA [6], does not respond to these therapeutic interventions or develop drug resistance shortly after treatment [7]. Recent clinical studies found that P-glycoprotein (P-gp), a member of the ATP binding cassette transporter family, is highly expressed on lymphocytes [8] or synovial cells [7] in patients with refractory RA and/or high disease activity. Moreover, the inhibition or reduction of P-gp overcomes drug resistance and improves disease outcomes for refractory RA patients [7–9]. Therefore, overcoming drug resistance through regulating P-gp is a potential strategy for the treatment of refractory RA [8].

Total glucosides of paeony (TGP), the active fraction of the roots of *Paeonia lactiflora* pall, have desirable therapeutic effects in

treating RA and systemic lupus erythematosus without significant adverse effects [10, 11]. Since 1998, it has been approved by the State Food and Drug Administration of China for the treatment of RA [1]. However, the absolute bioavailability of paeoniflorin (the main active ingredient of TGP) is only 3%–4% [12, 13], resulting in a slow onset of action and a limited response in RA patients after the oral administration of TGP [14, 15]. P-gp-mediated efflux is one of the major reasons for the low oral bioavailability of TGP [15, 16]. Therefore, new strategies to overcome P-gp-mediated efflux and increase the bioavailability of TGP are essential for boosting its therapeutic effect.

Nobiletin (5,6,7,8,3',4'-hexamethoxyflavone, C₂₁H₂₂O₈, Fig. 1b), a flavone isolated from *Citrus* peels, has anti-inflammatory, anticancer, antioxidative, cardiovascular protective, and antimetabolic disorder effects [17]. Our previous research demonstrated that nobiletin (N) inhibited the function of P-gp and increased the accumulation of chemotherapeutic agents in P-gp-overexpressing cancer cells [18] and drug-resistant tumors [19]. Moreover, our preliminary data indicated that nobiletin enhanced the absorption of paeoniflorin in rats (data not shown). Therefore, N was used as a P-gp inhibitor in this study to enhance the bioavailability of TGP

¹State Key Laboratory of Quality Research in Chinese Medicines, Macau University of Science and Technology, Taipa, Macao SAR, China; ²Faculty of Chinese Medicines, Macau University of Science and Technology, Taipa, Macao SAR, China; ³School of Pharmacy, Macau University of Science and Technology, Taipa, Macao SAR, China and ⁴Joint Laboratory for Translational Cancer Research of Chinese Medicine of the Ministry of Education of the People's Republic of China, School of Chinese Medicine, Guangzhou University of Chinese Medicine, Guangzhou 510006, China

Correspondence: Hua Zhou (hzhou@must.edu.mo) or Ying Xie (yxie@must.edu.mo)

Received: 18 August 2021 Accepted: 19 October 2021

Published online: 6 December 2021

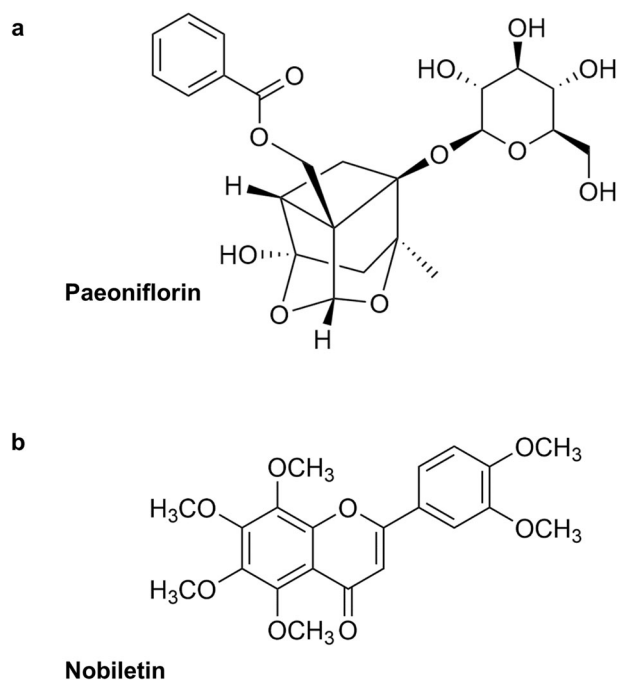


Fig. 1 The Chemical structures of paeoniflorin and nobiletin. **a** Paeoniflorin accounts for 45% of the active components and major pharmacological effects of total glucosides of paeony (TGP). **b** Nobiletin was used as a P-gp inhibitor.

and overcome drug resistance in P-gp-overexpressing lymphocytes to improve the therapeutic effects on refractory RA.

As a vital strategy for the delivery of poor aqueous drugs, self-nanoemulsifying drug delivery systems (SNEDDSs) are well known for their potential to enhance transcellular permeability and lymphatic transport, which exactly meets our goals [20–22]. Moreover, it forms an oil/water (O/W) emulsion, which is suitable for transporting hydrophilic TGP and hydrophobic nobiletin under mild agitation in gastrointestinal fluid [20]. In addition, SNEDDS also has other beneficial features, such as inhibiting efflux pumps, reducing first-pass metabolism, and rapidly diffusing through nanoemulsions [23–26]. Therefore, SNEDDS is a desirable drug delivery system for the codelivery of TGP and N to increase the bioavailability of TGP and develop a novel therapeutic strategy for patients with refractory RA.

Therefore, the purpose of this study was to develop a novel strategy for treating refractory RA by inhibiting P-gp to overcome drug resistance in P-gp-overexpressing lymphocytes and to enhance the overall bioavailability and effects of TGP in a refractory rat model. The TGP-N coloaded SNEDDS oral delivery system was developed and evaluated with an in vitro cell model, an in situ single-pass rat intestinal perfusion model, and in vivo PK-PD studies. Moreover, its ability to overcome drug resistance was also investigated in vitro with P-gp-overexpressing lymphocytes and in vivo with adjuvant-induced arthritis (AIA) model, which was verified for the overexpression of P-gp in lymphocytes and resistance to methotrexate (MTX) treatment at the same dosages that exhibited anti-inflammatory effects in normal lymphocytes.

MATERIALS AND METHODS

Chemicals and reagents

Total glucosides of paeony (TGP, containing 45.29% paeoniflorin, Fig. 1a, and 10.58% albiflorin) were obtained from Ningbo Yicuijian Biological Technology Co., Ltd, Ningbo, China. Nobiletin (purity $\geq 98.0\%$), paeoniflorin (purity $\geq 98.0\%$), albiflorin (purity

$\geq 98.0\%$), cremophor EL35 (EL 35), verapamil (VER), polyethylene glycol 400 (PEG), propanediol (Pol), polysorbate 20 (TWEEN 20, P20) and polysorbate 80 (TWEEN 80, P80) were purchased from Dalian Meilun Biotechnology Co., Ltd. Methotrexate was obtained from TCI Shanghai. Formic acid was provided by Fisher Scientific. Capryol 90, labrafil PG, labrafac lipophile WL1349, labrafil M2125CS, labrafil M1944CS, lauroglycol 90, lauroglycol FCC, labrasol, transcutool HP, maisine 35-1, and peceol were provided by France Gattefossé. HPLC-grade methanol was acquired from Merck (Darmstadt, Germany). ELISA kits for IL-6 were purchased from R&D Systems, and TNF- α and IL-1 β were purchased from Invitrogen Thermo Fisher Scientific. Primary antibodies against total AKT, HIF-1 α , and phosphorylated P-gp were obtained from Cell Signaling Technology. All other chemicals and reagents were of analytical grade or higher and were purchased through commercial sources.

Caco-2 and human monocyte THP-1 cell lines were obtained from ATCC (Passage 20–25, American Type Culture Collection, Rockville, MD, USA). The THP-1-P-gp cell line overexpressing P-gp was created by transfecting a plasmid containing the human ABCB1 (MDR1, P-gp) gene into the THP-1 cell line. Caco-2 cells were cultured at 37 °C and 5% CO₂ in Dulbecco's modified Eagle's medium. THP-1 and THP-1-P-gp cells were cultured at 37 °C with 5% CO₂ in RPMI-1640 medium.

UPLC–MS/MS analysis

UPLC–MS/MS was performed with a Waters ACQUITY UPLC™ (Waters, USA) system, and a 4000 QTRAP™ (AB science, America) mass spectrometer was used for the analysis of paeoniflorin, albiflorin, and N with a C₁₈ column (Waters ACQUITY UPLC® BEH C₁₈ Column, 2.5 μ m, 3.0 \times 100 mm, Waters Corp., Ireland). The mobile phases were composed of methanol and 0.1% formic acid at a flow rate of 0.35 mL/min. The developed UPLC–MS/MS method was validated within the concentration range of 5 ng/mL to 2500 ng/mL ($r^2 = 0.9993$) for paeoniflorin, 5 ng/mL to 2500 ng/mL ($r^2 = 0.9997$) for albiflorin, and 20 ng/mL to 1000 ng/mL ($r^2 = 0.9992$) for nobiletin. The precision, accuracy, stability, recovery, and matrix effect data are shown in Supplementary Tables 1–3, and representative chromatograms are illustrated in Supplementary Fig. 1.

SNEDDS for the codelivery of TGP and nobiletin

Equilibrium solubility test. The solubility of TGP and N in various oils (peceol, maisine, capryol 90, lauroglycol 90, labrafil PG, lauroglycol FCC, labrafac lipophile WL1349, labrafil M1944CS, labrafil M2125CS), surfactants (cremophor EL35, polysorbate 80, polysorbate 20, L90) and cosurfactants (transcutol HP, polyethylene glycol 400, L90, LFCC, WL1349, M1944CS, M2125CS, propanediol) were evaluated with the equilibrium method (shake-flask technique). Briefly, an excess amount of TGP or N was added to each tube containing 1 g of the selected excipients (oils, surfactant or cosurfactant). The mixture was vortexed for 10 min to obtain a homogeneous mixture and shaken to reach equilibrium at 37 °C for 72 h. Then, the mixture was centrifuged at 14000 r/min for 10 min to remove undissolved TGP and N. The concentrations of TGP or N in the supernatant were measured by UPLC–MS/MS after appropriate dilution.

Screening of the surfactant and cosurfactant with an emulsification study. Emulsification studies were performed to screen the suitable surfactant with the selected oil [27]. Briefly, 300 mg of surfactant was added to 300 mg of selected oil (Cap 90). The mixture was vortexed for 5 min and then heated at 45 °C for 30 s to form an isotropic mixture before further dilution with deionized water.

Cosurfactants were compared for their ability to improve the emulsification of the selected surfactant and oil. The selected surfactant (0.3 g, EL 35) was mixed with the tested cosurfactants

(0.2 g) followed by the addition of the oily phase (0.5 g, caprol 90). The mixture was vortexed for 5 min and then heated at 45 °C for 30 s to form an isotropic mixture before further dilution with deionized water to yield a fine emulsion.

The drop size and transmittance for each emulsion generated with different surfactants and cosurfactants were evaluated. The transmittance of emulsions was measured at 638 nm with a 96-well plate microplate reader [27]. The droplet size distribution and polydispersity index (PDI) of the emulsions were detected using a Malvern Zetasizer Nano ZS90 instrument (Malvern Instruments Ltd., Malvern, UK) at 25 °C.

Pseudoternary phase diagram. To identify the nanoemulsion area, different formulations containing the oil phase (Cap 90), surfactant (EL35), and cosurfactant (PEG or THP) were constructed to form a pseudoternary phase diagram. The ratios of surfactant/cosurfactant (K_m) were 1:1, 2:1, and 3:1. The mixture of surfactant and cosurfactant was further mixed with the oil phase at ratios of 1:9 to 9:1 (w/w) at 500 r/min for 1 h (37 °C). Then, the final mixture was titrated with deionized water at 500 r/min and 37 °C (IKA RT-5 multiposition magnetic stirrer). The self-emulsifying properties of SNEDDS were visually observed to delineate the boundary of the nanoemulsion area in the pseudoternary phase diagram.

Preparation of SNEDDS for the codelivery of TGP and N
The formulations were prepared by mixing oil with a mixture of surfactant and cosurfactant at the optimized K_m ratio. TGP and N were accurately weighed into a 500 mL round bottom flask and dissolved in 100 mL of ethanol by sonication for 1 h. Subsequently, the selected oil, surfactant and cosurfactant were added to the drug solution. The resulting formulation was mixed, and ethanol was removed by a rotary evaporator under vacuum at 60 °C for two hours. The final formulations were subject to further characterization.

In vitro evaluation of TGP-N-SNEDDS

Droplet size, transmittance, PDI, and zeta-potential measurements. The droplet size, transmittance, and PDI of the optimized SNEDDS formulation were determined with the methods described in Section 2.3.2. Zeta potential measurements were performed with a Malvern Zetasizer Nano ZS90 instrument (Malvern Instruments Ltd., Malvern, UK) and a 100-fold dilution of the optimized SNEDDS.

Cloud point analysis. The SNEDDS formulation was diluted 100-fold with deionized water and gentle stirring at 37 °C before gradually increasing the temperature. When turbidity suddenly appeared, the temperature was recorded as the cloud point. This experiment was carried out in triplicate.

Thermodynamic stability. Thermodynamic stability studies were carried out under different conditions, including heating (45 °C for 48 h)–cooling (4 °C for 48 h) cycles, centrifugation (3500 r/min for 0.5 h) and freezing (–20 °C for 48 h)–thawing (25 °C for another 48 h) cycles [28].

Transmission electron microscopy (TEM). After dilution with deionized water, the nanoemulsion was dropwise added to a carbon film-coated copper mesh and dried naturally. After staining with 2% w/v phosphor-tungstic acid solution for negative staining, the dried samples were observed with a transmission electron microscope (FEI Tecnai G2 20, USA) to obtain the morphology of SNEDDS.

Influence of dilution on SNEDDS stability. The influence of dilution on the stability of SNEDDS was also assessed by diluting the formulation 10-, 20-, 50-, 100-, 500-, and 1000-fold with deionized water. The particle size of the diluted TGP-N-SNEDDS

was determined using a Malvern Zetasizer Nano ZS90 at 25 °C. Moreover, we also evaluated the stability of CEP and CET in simulated intestinal fluid (pH 6.8) and simulated gastric fluid (pH 1.2).

In vitro drug release. The in vitro drug release of SNEDDS was conducted with the dialysis method [29]. Briefly, SNEDDS was put in an activated dialysis membrane (MWCO 7000 Da, Viskase, USA) and immersed in 900 mL of release medium (PBS, pH 7.4) containing 0.1% P 80 (w/v) with stirring at 100 r/min and a temperature of 37 ± 0.5 °C. The dissolution medium (1 mL) was withdrawn at predetermined time intervals over 12 h, and then an equal volume of fresh medium was added. The concentration of paeoniflorin was determined by UPLC–MS/MS after dilution.

In situ single-pass rat intestinal perfusion studies

Sprague–Dawley (SD) rats (250 ± 20 g) were housed six per cage and acclimated for 7 days in a 12 h light/dark cycle room at 25 ± 2 °C with standard animal feed. All the SD rats were deprived of food overnight before the experiment but were allowed free access to water.

All animal studies were approved by the Animal Care and Use Committee at Guangzhou University of Chinese Medicine (No # ZYLL20150807) and carried out following the “Institutional Animal Care and User Committee Guidelines”.

An in situ single-pass intestinal perfusion model was used to study the intestinal absorption of drugs in rats [30, 31]. The rats were fasted for 24 h with free access to water and then randomly divided into four groups ($n = 6$): TGP, TGP + N, Cap 90- EL35-PEG (CEP), and Cap 90-EL35-THP (CET) groups. Briefly, after anesthesia with thiopental sodium (50 mg/kg), an incision was made in the middle line of the abdomen to expose the small intestine. Four intestinal sections were isolated and cannulated, including the duodenum, jejunum, ileum, and colon. After rinsing with normal saline at 37 °C for 30 min, a perfusion solution containing target drugs or formulations (40 mg/L TGP for all four groups) was connected to each segment and perfused through each part of the four intestine sections by using a perfusion pump (Harvard Apparatus, Cambridge, MA) at a flow rate of 0.167 mL/min. The perfusate samples were collected from the outlet cannula within 2 h and analyzed by UPLC–MS/MS. The effective permeability coefficient (P_{eff}) and the percent absorption rate of paeoniflorin of the four intestinal segments were calculated.

In vitro transport study with Caco-2 cells

We investigated the transport of the SNEDDS over a Caco-2 monolayer cell model based on the reported method with modification [32] by evaluating the permeability of target compounds or formulations from the apical to basolateral (AP-BL) direction or from the basolateral to apical (BL-AP) direction at 37 °C with gentle shaking. Before the transport study, the culture medium was replaced with preheated Hank’s balanced salt solution (HBSS). For the AP-BL transport study, the apical side was 0.5 mL HBSS containing test drugs, and the other side was 1.5 mL of blank HBSS. For the BL-AP transport study, the basolateral side was 1.5 mL of HBSS containing test drugs, and the apical side was 0.5 mL of blank HBSS. Samples from the AP (BL-AP) or BL (AP-BL) side solution were collected at 30, 60, 90, and 120 min and then replenished with an equal volume of blank HBSS. The samples were subjected to UPLC–MS/MS analysis for the quantification of paeoniflorin. The apparent permeability coefficient (P_{app}) and efflux ratio were calculated as we previously described [32].

Pharmacokinetic study

Rats were randomly divided into four groups ($n = 6$): TGP (150 mg/kg), TGP (150 mg/kg) + N (100 mg/kg), SNEDDS formulation 1 (CEP) and SNEDDS formulation 2 (CET) with equal dosages of TGP

and N. After oral administration, a 100 μ L blood sample was collected via the tail vein at 0.083, 0.25, 0.5, 1, 2, 3, 4, 6, 8, 10, and 12 h, with a heparinized tube before centrifugation at 6000 r/min for 10 min. The plasma samples were stored at -80°C prior to LC–MS measurement.

DAS 2.0 software (version 2.0, Drug and Statistics, China) was used to calculate the pharmacokinetic parameters, including the mean residence time (MRT), maximum plasma concentration (C_{max}), time to reach the maximum plasma concentration (T_{max}), half-life ($t_{1/2z}$), area under the plasma concentration-time curve to the last time or infinity ($\text{AUC}_{(0-t)}$ or $\text{AUC}_{(0-\infty)}$) and clearance ($\text{CL}_{z/F}$).

P-gp-overexpressing THP-1 cells (THP-1-P-gp) and THP-1 cells were seeded in 6-well plates (10^6 cells/well) in RPMI-1640 medium containing 100 nM PMA for 24 h. Medium containing TGP, TGP + N, TGP + verapamil (a typical P-gp inhibitor), the CEP formulation, or the CET formulation was added and incubated for 4 h. After 4 h, the supernatant was removed, and the attached cells were washed three times with cold PBS before lysis with 1% v/v Triton X-100 solution. Then, methanol was added to each cell lysis solution, and the mixture was centrifuged at 4°C and 14,000 r/min for 20 min. The supernatant was subjected to UPLC–MS/MS analysis for the quantification of paeoniflorin.

RT–PCR

Cells were pretreated with 100 nM PMA for 24 h and then incubated with different drugs for 22 h before stimulation with LPS (10 ng/mL) for 2 h. After treatment, the cells were collected with TRIzol reagent (InvitrogenTM), and chloroform was added before centrifugation at 12,700 r/min for 20 min at 4°C . Isopropanol (400 μ L) was added to the supernatant and frozen at -40°C for 30 min. After centrifugation at 12,700 r/min for 40 min, the precipitated RNA was suspended in 1 mL of 75% ethanol and centrifuged at 12,700 r/min for 5 min at 4°C . The purity and amount of RNA in each sample were evaluated by Nanodrop One (Gene Company Limited). cDNA synthesis was carried out according to the manufacturer's instructions for the cDNA synthesis kit (Accurate Biotechnology).

The primer sequences were as follows: F-5'-GAGCCAGTCCCTC-TATTATG-3', R-5'-AGGGCGATTACAGACACAAC-3' for TNF α , F-5'-CATTGCTCAAGTGTCTGAAGC-3', R-5'-CATGGCCACAACAAGTACG-3' for IL-1 β , F-5'-ACTCACCTCTCAGAACGAATTG-3', R-5'-CCATCTT TGGAAAGTTCAGGTTG-3' for IL-6, and F-5'-CATGTACGTTGCTAT CCAGGC-3', R-5'-CTCCTTAATGTCACGCACGAT-3' for β -actin. The results of quantitative real-time PCR were evaluated by a ViiATM 7 real-time quantitative PCR system and expressed with comparative $\Delta\Delta\text{Ct}$ values normalized to the levels of β -Actin.

Adjuvant-induced arthritis rat model

Adjuvant-induced arthritis (AIA) of rats was induced by injection of complete Freund's adjuvant. Briefly, 100 μ L of heat-killed *Mycobacterium tuberculosis* in mineral oils was intradermally injected into the left hind paw of SD rats (100–120 g) [33–35]. Then, the rats were randomly divided into 7 groups on Day 9 after injection ($n = 6$), including the normal group (PBS as vehicle), model group (PBS as vehicle), MTX 0.5 mg/kg group (MTX-L, 0.5 mg/kg every 3 days) [34], MTX 7.6 mg/kg group (MTX-H, 7.6 mg/kg per week), TGP group (150 mg/kg per day), TGP (150 mg/kg per day) + N group (100 mg/kg per day), and CET formulation group (containing TGP 150 mg/kg per day + N 100 mg/kg per day).

The body weight, paw volumes, and arthritis index scores were measured every two days. Arthritis severity was graded with clinical scores according to traditional methods [36]. On Day 30 after treatment, the rats were sacrificed, and the right hind paw was amputated for histological examination via hematoxylin and eosin (H&E) staining and micro-CT scanning (SkyScan 1176, Bruker, Belgium) to visualize bone erosion. Rat serum was used to measure cytokines, including TNF- α , IL-6, and IL-1 β , according to the manufacturer's instructions. Lymphocytes isolated from the

peripheral blood of two AIA rats were combined into one sample to determine the intracellular paeoniflorin concentration and to perform Western blot assays.

Resistant evaluation in lymphocytes from AIA rats

To evaluate the expression of P-gp, rat lymphocytes were prepared according to the manufacturer's instructions (Ficoll-Paque PREMIUM, GE Healthcare Bio-Sciences AB) and identified by CytoFLEX flow cytometers. Blood lymphocytes (2×10^5 cells) were collected and incubated with APC/Cyanine7 anti-rat CD45, APC anti-rat CD3, and MDR1 PE antibodies for 30 min at 4°C before being suspended in PBS for flow cytometry.

Moreover, to evaluate the overcoming effects, lymphocytes were isolated from the control and AIA model group rats according to a previously described method [37]. After resuspension in RPMI-1640 medium containing 10% fetal bovine serum (FBS), the lymphocytes were incubated with test compounds and 1 μ g/mL LPS for 36 h. At the end of the experiment, cell viability ($\geq 90\%$) was detected by using trypan blue dye exclusion. After 36 h, lymphocytes were collected and centrifuged at $500 \times g$ for 10 min. Cytokines, including TNF- α , IL-6, and IL-1 β , were analyzed with the supernatants, while pellets were used for Western blot assay and the determination of intracellular content of paeoniflorin in terms of TGP.

Western blot analysis

Cells were lysed with RIPA buffer containing protease and phosphatase inhibitors (Roche Life Science, USA). A Bio-Rad protein assay was used to measure the protein concentration. Equal amounts of protein were loaded on SDS–PAGE gels and blotted onto methanol-activated PVDF membranes (Millipore, Darmstadt, Germany). After incubation with a blocking solution containing 5% (w/v) bovine serum albumin in TBST buffer (10 mM Tris, pH 7.4, 0.9% NaCl, and 0.1% Tween 20) for 1.5 h at room temperature, the membrane was incubated with primary and secondary antibodies and subsequently visualized with an Immobilon[®] western chemiluminescent substrate detection kit (Millipore, USA). GAPDH was used as the loading control for the WB assays.

Statistical analysis

Data were expressed as the mean \pm standard deviation (SD). Statistical analysis was performed with one-way analysis of variance (ANOVA) by using GraphPad Software (Prism9, San Diego, CA, USA). A $P \leq 0.05$ is statistically significant.

RESULTS

Solubility and emulsification ability evaluation

We first compared the solubility of TGP and N in different oils, surfactants, and cosurfactants. Both TGP and N showed the highest solubility in caprol 90 (Cap 90), which was 101.68 mg/g and 52.80 mg/g, respectively, as shown in Fig. 2a. Considering that the solubility in the oil phase is a key factor for SNEDDS formulation, Cap 90 was selected as the oil phase.

To screen suitable surfactants, we compared their emulsification ability with oil phase Cap 90. Nonionic surfactants were used in this study for their safety and stability at different pH values and ionic strengths [38]. As shown in Group A of Table 1, we compared the emulsifying ability of EL 35, P80, P 20, labrasol, and L90 with that of Cap 90 based on parameters including particle size, PDI, and transmittance. Among these surfactants, EL35 showed the best emulsification ability with Cap 90, with the desired particle size (92.00 ± 1.76 nm) and highest transmittance (92.21 ± 0.15) observed. Therefore, EL35 was selected as the surfactant for further investigation.

Next, we compared the compatibility of the cosurfactant (THP, PEG, L90, LFCC, WL1349, M1944CS, M2125CS, and Pol) with the selected surfactant EL35 and oil Cap 90. As shown in Group B of Table 1, both PEG and THP have a relatively high emulsifying

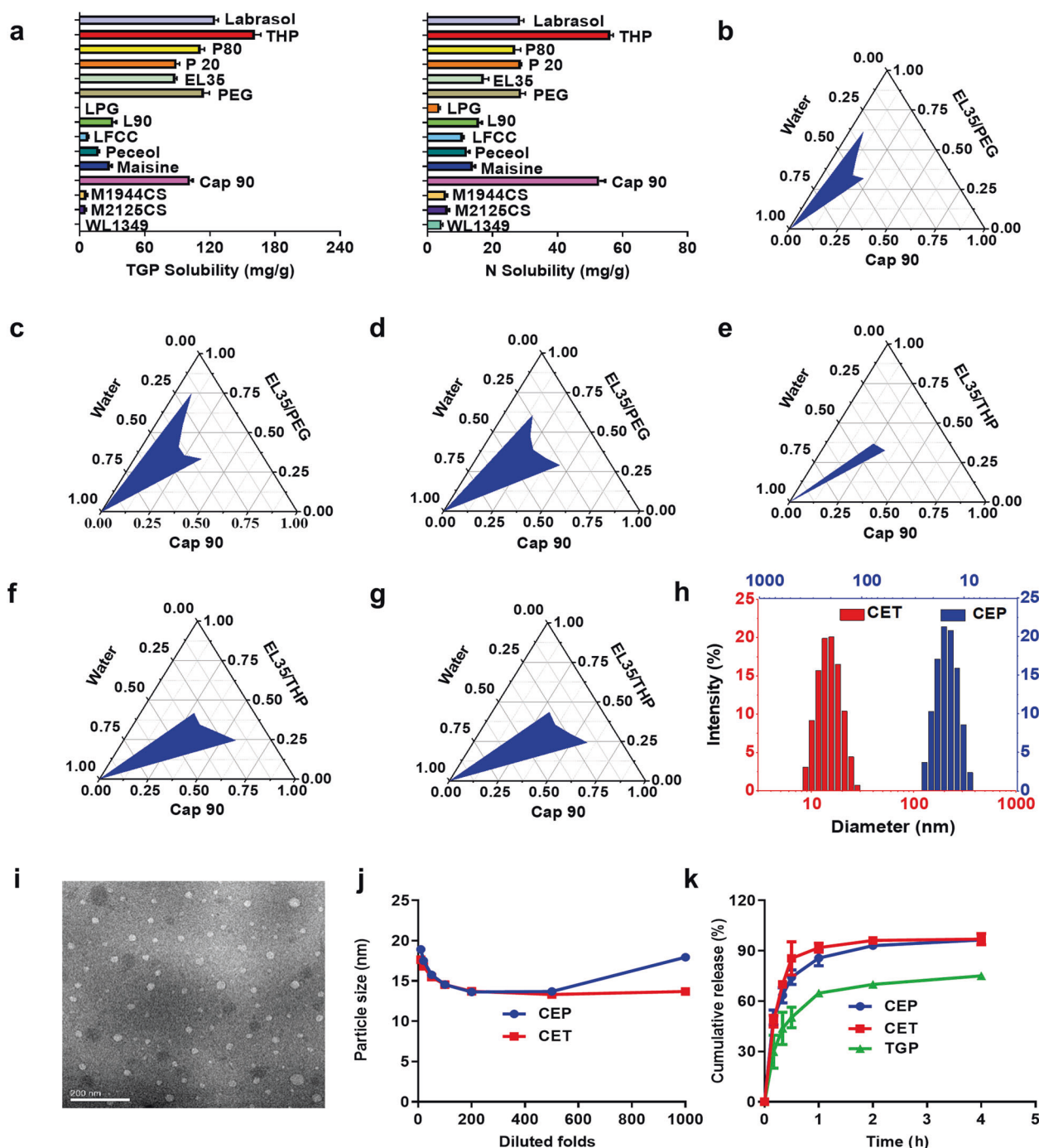


Fig. 2 Development and in vitro evaluation of the optimized SNEDDS formulations. **a** Solubility of total glucosides of paeony (TGP) and nobiletin (N) in different excipients, including labrafil PG (LPG), lauroglycol 90 (L90), lauroglycol FCC (LFCC), peceol, maisine, capryol 90 (Cap 90), labrafil M1944CS (M1944CS), labrafil M2125CS (M2125CS), labrafac lipophile WL1349 (WL1349), labrasol, propanediol (Pol), polysorbate 80 (P80), polysorbate 20 (P 20), transcitol HP (THP), cremophor EL35 (EL35) and polyethylene glycol 400 (PEG). Pseudoternary phase diagrams were constructed for formulation 1, which was composed of Cap 90, EL35, and PEG (**b–d**), and formulation 2, which was composed of Cap 90, EL35, and THP (**e–g**). The ratio of surfactant and cosurfactant (K_m) was evaluated at 1:1 (**b** and **e**), 2:1 (**c** and **f**), and 3:1 (**d** and **g**). The blue area represents the O/W nanoemulsion existence region. **h** Particle sizes of formulation 1 Cap 90-EL35-PEG (CEP, blue) and formulation 2 Cap 90-EL35-THP (CET, red). **i** Typical TEM images of CET. **j** Particle size profiles of CET and CEP after dilution with water (10–1000-fold) ($n = 3$). **k** In vitro cumulative release profiles of TGP (shown with the content of paeniflorin) from CEP or CET compared with TGP ($n = 3$). All data are presented as the mean \pm SD.

efficiency with Cap 90 (in 20%) in the presence of EL35 (in 30%). In addition, TGP and N have a high solubility in PEG or THP, as displayed in Fig. 2a. Consequently, PEG and THP were selected as cosurfactants for designing the SNEDDS formulation to codeliver TGP and N.

Construction of pseudoternary phase diagrams
To determine the self-emulsification region and the optimal composition of SNEDDS in the absence of TGP and N, pseudoternary phase diagrams were constructed by mixing the appropriate amounts of Cap 90 with a mixture of surfactant and

Table 1. Optimization of SNEDDS formulations ($n = 3$).

Group*	Oil (%)	Surfactant (%)	Co- Surfactant (%) ^a	Particle (nm)	PDI	Transmittance (%) ^a
A	50% Cap 90	50% EL35	—	92.00 ± 1.76	0.330 ± 0.009	92.21 ± 0.15
A	50% Cap 90	50% P 80	—	137.07 ± 5.95	0.517 ± 0.020	76.13 ± 1.69
A	50% Cap 90	50% P 20	—	981.3 ± 78.9	0.960 ± 0.069	69.66 ± 5.37
A	50% Cap 90	50% Labrasol	—	347.6 ± 14.6	0.439 ± 0.028	35.13 ± 4.52
A	50% Cap 90	50% L90	—	8168 ± 485.4	0.739 ± 0.045	91.29 ± 1.09
B	50% Cap 90	30% EL35	20% THP	75.21 ± 1.02	0.113 ± 0.009	96.89 ± 0.22
B	50% Cap 90	30% EL35	20% PEG	76.47 ± 1.07	0.117 ± 0.014	96.54 ± 0.14
B	50% Cap 90	30% EL35	20% Pol	77.23 ± 1.60	0.116 ± 0.016	97.01 ± 0.11
B	50% Cap 90	30% EL35	20% L90	96.28 ± 0.51	0.200 ± 0.019	80.75 ± 1.12
B	50% Cap 90	30% EL35	20% LFCC	67.72 ± 1.86	0.235 ± 0.012	90.72 ± 1.00
B	50% Cap 90	30% EL35	20% WL1349	61.25 ± 0.14	0.173 ± 0.004	95.59 ± 0.14
B	50% Cap 90	30% EL35	20% M1944CS	46.05 ± 0.35	0.076 ± 0.016	98.44 ± 0.09
B	50% Cap 90	30% EL35	20% M2125CS	45.18 ± 0.61	0.061 ± 0.006	98.39 ± 0.17
C	10% Cap 90	67.5% EL35	22.5% PEG	13.37 ± 0.09	0.017 ± 0.003	—
C	13% Cap 90	65.25% EL35	21.75% PEG	13.81 ± 0.02	0.020 ± 0.004	—
C	15% Cap 90	63.75% EL35	21.25% PEG	14.52 ± 0.10	0.028 ± 0.006	—
C	17% Cap 90	62.25% EL35	20.75% PEG	15.57 ± 0.14	0.042 ± 0.004	—
C	18% Cap 90	61.5% EL35	20.5% PEG	16.16 ± 0.13	0.047 ± 0.006	—
C	19% Cap 90	60.75% EL35	20.25% PEG	18.51 ± 0.25	0.128 ± 0.015	—
C	20% Cap 90	60% EL35	20% PEG	36.85 ± 2.00	0.522 ± 0.040	—
C	30% Cap 90	52.5% EL35	17.5% PEG	111.3 ± 3.78	0.417 ± 0.083	—
D	10% Cap 90	67.5% EL35	22.5% THP	13.39 ± 0.05	0.017 ± 0.004	—
D	13% Cap 90	65.25% EL35	21.75% THP	13.86 ± 0.09	0.011 ± 0.003	—
D	15% Cap 90	63.75% EL35	21.25% THP	14.55 ± 0.13	0.027 ± 0.006	—
D	17% Cap 90	62.25% EL35	20.75% THP	15.68 ± 0.14	0.038 ± 0.008	—
D	18% Cap 90	61.5% EL35	20.5% THP	16.27 ± 0.20	0.046 ± 0.007	—
D	19% Cap 90	60.75% EL35	20.25% THP	18.65 ± 0.26	0.135 ± 0.022	—
D	20% Cap 90	60% EL35	20% THP	38.38 ± 1.23	0.515 ± 0.026	—
D	30% Cap 90	52.5% EL35	17.5% THP	79.39 ± 1.53	0.642 ± 0.018	—

Notes: *Group A for comparing the compatibility of surfactants (labrasol, polysorbate 80 (P80), polysorbate 20 (P 20), lauroglycol 90 (L90), and cremophor EL35 (EL35)) with oil phase Cap 90.

*Group B for comparing the compatibility of co-surfactants (transcutol HP (THP), propanediol (Pol), lauroglycol FCC (LFCC), L90, polyethylene glycol 400 (PEG), labrafil M1944CS (M1944CS), labrafil M2125CS (M2125CS), and labrafac lipophile WL1349 (WL1349)) with EL35 and Cap 90.

*Group C for evaluating the effects of oil percentages on the particle size and PDI of SNEDDS formulations composited with EL35 and PEG400.

*Group D for evaluating the effects of oil percentages on the particle size and PDI of SNEDDS formulations composited with EL35 and THP.

^a " —": Not detected.

cosurfactant at ratios from 1:9 to 9:1 (w/w). The ratio of surfactant and cosurfactant (K_m) was set to 1:1 (Fig. 2b and e), 2:1 (Fig. 2c and f), and 3:1 (Fig. 2d and g), respectively. As shown in Fig. 2b–g, we found that as K_m increased, the area of the nanoemulsion increased. Therefore, the optimal ratio of EL35/PEG or EL35/THP in SNEDDS was $K_m = 3:1$.

In the C and D groups of Table 1, when the percentages of the oil phase were below 19%, the particle sizes were between 13.37–18.65 nm, and the PDI values were below 0.14. However, if the percentage of oil was $\geq 20\%$, the PDI increased rapidly to above 0.2, and the particle size increased to approximately 100 nm. Therefore, due to the increased oil-water boundary area, the smaller the particle size and PDI achieved, the more stable the SNEDDS system will be [39]. Hence, the percentages of the oil phase should be below 19% to obtain a more stable SNEDDS. However, SNEDDS formulations with a low oil content ($\leq 10\%$) exhibited a limited ability for improving drug bioavailability [40]. Therefore, 15% oil was used as the optimized SNEDDS system with a mixture of EL35 and PEG or THP at $K_m = 3:1$.

The maximum drug loading ability of TGP and N in the optimized SNEDDS was 64.95 mg/g and 30.56 mg/g for formulation one

composed of Cap 90-EL35-PEG (CEP) and 63.85 mg/g and 30.71 mg/g for formulation two composed of Cap 90-EL35-THP (CET), respectively.

In vitro characterization of TGP-N-loaded SNEDDS
Thermodynamic stability and cloud point. Both SNEDDS formulations (CEP and CET) showed good stability without phase separation in thermodynamic stability tests after heating, centrifugation, and freeze-thaw cycles.

Moreover, phase separation in the gastrointestinal tract has a negative impact on drug absorption. To avoid the phase separation of SNEDDS in the gastrointestinal tract, the cloud point of SNEDDS should be above 37 °C [41]. Here, we found that the cloud points of the prepared CEP and CET nanoemulsions were 74 °C and 77 °C, respectively, indicating that they were stable at body temperature.

Droplet size, PDI, and Zeta potential measurements. We also evaluated the PDI, which represents the uniformity of SNEDDS formulations. The mean particle sizes were 14.54 ± 0.07 nm for CET

and 14.52 ± 0.05 nm for CEP, as shown in Fig. 2h. The PDI values were 0.038 ± 0.004 for CET and 0.027 ± 0.006 for CEP, which is far below 0.5, indicating the uniformity of the globule size distribution. Moreover, the zeta potentials were -1.44 ± 0.14 mV for CET and -1.73 ± 0.06 mV for CEP. All these data suggest that the two SNEDDS formulations produced transparent emulsions of nanometric size.

Transmission electron microscopy (TEM) analysis. To image the morphology and capture microstructural transitions, the CET formulation was analyzed with TEM after dilution with deionized water. As shown in Fig. 2i, the typical TEM image illustrated that the CET formulation had spherical globules in appearance and was distributed evenly in clear surroundings. No drug precipitation or coalescence was observed, indicating the stability of the reconstituted dispersion. In addition, the emulsion size was ~ 20 nm, which was consistent with the particle size results described above.

Dilution robustness. Since the diluent may affect the self-emulsification stability of SNEDDS and lead to drug precipitation, the stability of formulations CEP and CET were evaluated at different dilution factors to simulate the in vivo gradual dilution conditions. After 10-1000-fold dilution, the particle sizes of CEP and CET SNEDDS were within 10–20 nm, as shown in Fig. 2j and Supplementary Fig. 5. In addition, no signs of phase separation or drug precipitation were observed for the obtained nanoemulsions after 12 h, suggesting that these two formulations were stable after aqueous dilution.

In vitro drug release. In Fig. 2k, the accumulative release of paeoniflorin from formulations exceeds 95% within 1 h. The release rates of paeoniflorin in the two formulations were much higher than that of TGP due to the small particle size of SNEDDS, indicating a larger surface area for drug release.

In situ intestinal absorption

To investigate the permeability and absorption of the CET formulation in the small intestine, an in situ single-pass intestinal perfusion (SPIP) model was used to evaluate the intestinal permeability (P_{eff}) of the target compound. Both SNEDDS formulations (CEP and CET) significantly increased the absorption of TGP (paeoniflorin) in four intestinal segments (duodenum, jejunum, ileum, and colon), with $P < 0.001$, as shown in Fig. 3a. Moreover, CET showed higher efficacy in increasing the permeability of TGP than CEP. Additionally, our data indicated that TGP (paeoniflorin) had the highest effective permeability in the duodenum ($P_{eff} = 0.110 \pm 0.018 \times 10^{-4}$ cm/s) and the lowest permeability in the colon ($P_{eff} = 0.090 \pm 0.012 \times 10^{-4}$ cm/s) of the four intestinal segments.

The absorption rates of TGP indexed with paeoniflorin in CEP and CET formulations were $3.36\% \pm 0.30\%$ and $4.08\% \pm 0.62\%$, respectively, which were higher than TGP in the vehicle (2.24%) in the SPIP model.

Caco-2 cell permeability studies

Next, we explored the effects of N or SNEDDS formulation on the transport of TGP over Caco-2 monolayer cells with the typical P-gp inhibitor verapamil used as a positive control. As shown in Fig. 3b, after TGP treatment, the P_{app} values of paeoniflorin were measured in both the apical to basolateral (A-B) and basolateral to apical (B-A) directions. The P_{app} (B-A) of paeoniflorin was much higher than that of P_{app} (A-B), with an efflux ratio of 3.98 ± 0.46 (Fig. 3c). If a compound has an efflux ratio of greater than 2, it suggests that the compound may be subject to active efflux [42]. Therefore, our data indicated the active efflux of TGP over intestinal cells. Verapamil significantly inhibited the efflux with efflux ratio (1.18 ± 0.15) and increased the transport of TGP from A to B, proving that active efflux of the major constituents in TGP was mediated by P-gp [43].

As we expected, the cotreatment of N with TGP reduced the efflux ratio of paeoniflorin to 1.06 ± 0.10 and significantly increased the transport of TGP from A to B. Notably, N was more efficient than verapamil in inhibiting the active efflux of paeoniflorin.

The efflux ratios decreased to 0.56 ± 0.03 for CET and 0.88 ± 0.10 for CEP, suggesting that both formulations inhibited intestinal active efflux. Moreover, CEP and CET formulations exhibited a higher permeability than that of the cotreatment of N with TGP. The P_{app} (A-B) values of the CET formulation increased by 4.67 ± 0.20 -fold compared with the TGP group and 2.04 ± 0.09 -fold compared with the TGP and N cotreatment group, suggesting that the CET formulation not only inhibited P-gp but also significantly increased the permeability of TGP over intestinal cells.

Pharmacokinetic study

A pharmacokinetic study was carried out to investigate the oral bioavailability of TGP after oral administration of CEP and CET SNEDDS formulations to rats. Mean plasma concentration-time profiles of paeoniflorin in rats are illustrated in Fig. 3d. After treatment with TGP in the vehicle, there was a short T_{max} (0.5 h) with a mean C_{max} of approximately 282.17 ± 76.26 ng/mL for paeoniflorin, indicating that TGP was absorbed quickly but was poorly absorbed, which was consistent with previous reports [12, 13].

Both CEP and CET formulations as well as the cotreatment with N significantly improved the absorption of TGP. As shown in Table 2, the AUC_{0-t} of paeoniflorin increased 4.35- and 3.96-fold after oral administration of CET and CEP compared with that of TGP alone, indicating the increased bioavailability of TGP in the formulations. The AUC of albiflorin (another major active compound in TGP) for CET and CEP formulations also increased, as shown in Supplementary Fig. 2. Interestingly, the plasma half-life $t_{1/2z}$ of paeoniflorin after administration of the CEP and CET formulations was 6.14- and 3.96-fold longer than that of the TGP groups. Additionally, the CL_z/F of paeoniflorin in the CET and CEP groups decreased by 16.01% and 25.65%, respectively. Furthermore, we noticed an increased AUC for N after treatment with the CET or CEP formulation (Supplementary Fig. 3). All these data indicated that SNEDDS improved the bioavailability of TGP and N with enhanced absorption and delayed excretion, suggesting that SNEDDS may lead to an improved therapeutic effect as well as duration of treatment.

Increased cellular accumulation and therapeutic effects in P-gp-overexpressing THP cells

To investigate whether CET formulations can overcome resistance by inhibiting the efflux induced by P-gp, we developed an overexpressing P-gp human THP-1 cell line (THP-1-P-gp). First, we evaluated the cellular accumulation of TGP (shown with the content of paeoniflorin) in THP-1-P gp cells in comparison with sensitive THP-1 cells. As shown in Fig. 4a, the content of paeoniflorin was significantly reduced in THP-1-P gp cells (-34.05%) compared with THP-1 cells, indicating a rise in drug efflux induced by P-gp. TGP and MTX consistently suppressed LPS-induced increases in TNF- α , IL-1 β , and IL-6 mRNA in THP-1 cells; however, they did not exhibit any anti-inflammatory effects in THP-1-P-gp cells at the same dosage (Fig. 4b and c), confirming that resistance to MTX and TGP was related to the overexpression of P-gp in lymphocytes.

The presence of verapamil, a specific inhibitor of P-gp, and N increased the intracellular concentration of TGP (paeoniflorin) in THP-1-P gp cells, suggesting the participation of P-gp in TGP efflux. Consistent with the increased accumulation of TGP, cotreatment with N or verapamil significantly reduced the mRNA expression levels of IL-6, TNF- α , and IL-1 β (-23.66% – 44.36%) in THP-1-P-gp cells. In contrast, N did not enhance the anti-inflammatory effects of TGP in sensitive THP-1 cells.

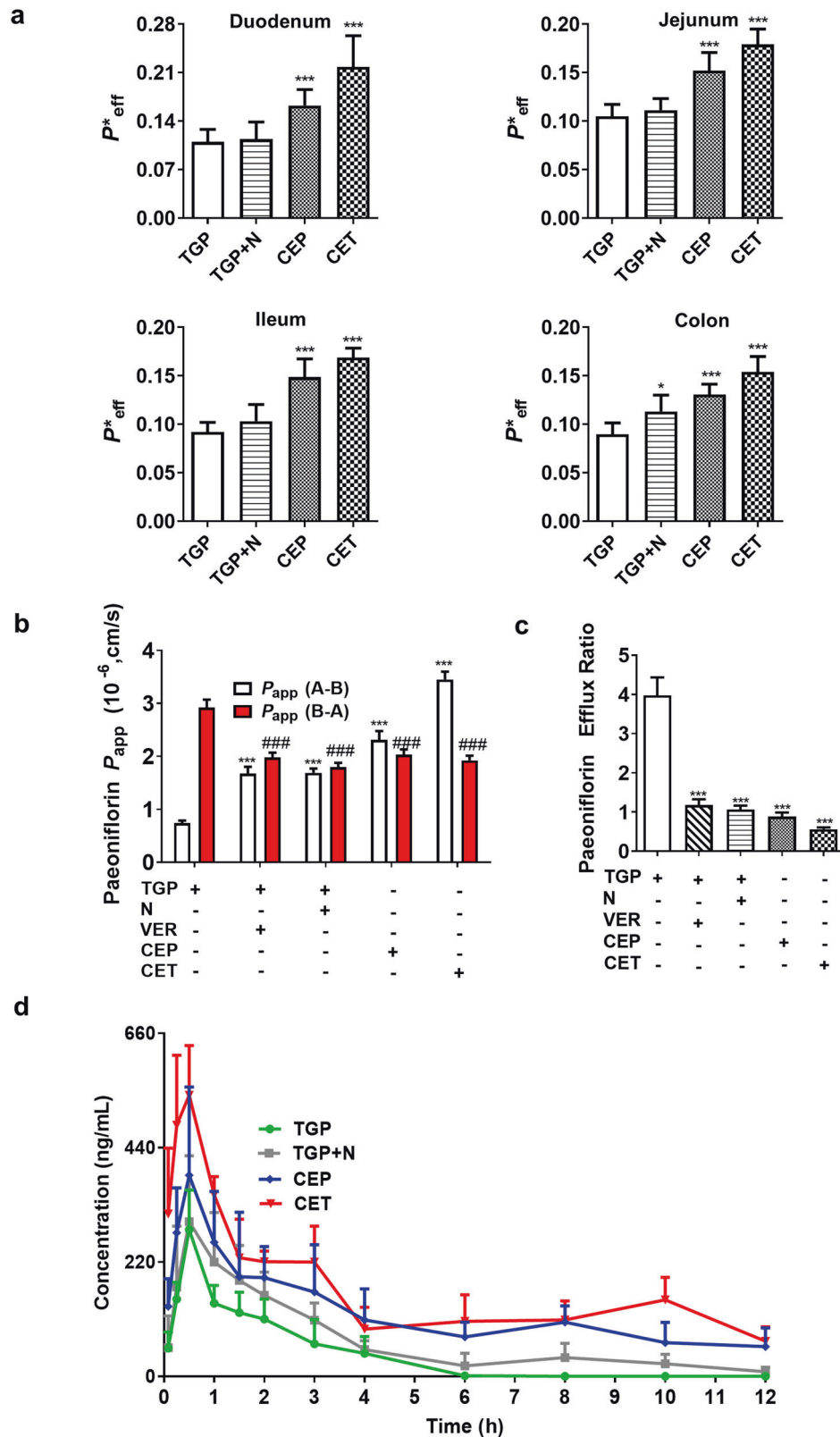


Fig. 3 Effective intestinal permeability of the SNEDDS formulations evaluated in the ex vitro intestinal perfusion model and Caco-2 cell monolayer model. **a** CEP and CET formulations were evaluated for their permeability over the duodenum, jejunum, ileum, and colon in the ex vitro intestinal perfusion model by comparison with TGP in the vehicle ($n = 6$). **b** The bidirectional apparent permeability (P_{app}) and **(c)** efflux ratio of TGP (paeoniflorin) were evaluated after two SNEDDS formulations were administered to Caco-2 cells and compared with TGP given alone ($n = 3$). The doses of TGP, verapamil (VER, positive control), and nobiletin (N) used in the Caco-2 experiments were 40.00, 18.18, and 26.67 $\mu\text{g}/\text{mL}$, respectively. **d** Mean plasma concentration-time profiles of paeoniflorin in rats after the oral administration of CEP, CET, TGP + nobiletin (N) or TGP in the vehicle ($n = 6$). Data expressed as the mean \pm SD. * $P < 0.05$, ** $P < 0.01$, *** $P < 0.001$, and ### $P < 0.001$, vs. the TGP alone group.

Table 2. Main pharmacokinetic parameters of paeoniflorin in rats after oral administration of SNEDDS formulations ($n = 6$).

Parameters	Unit	TGP	TGP+N	CEP	CET
AUC _(0-t)	μg/L·h	446.49 ± 74.46	820.34 ± 109.30*	1458.13 ± 168.77***##	1942.43 ± 257.80***##
AUC _(0-∞)	μg/L·h	484.83 ± 104.24	856.13 ± 120.84	1868.37 ± 337.93***##	3019.54 ± 612.15***##
MRT _(0-t)	h	1.51 ± 0.20	3.07 ± 0.85**	4.42 ± 0.90***#	4.51 ± 0.25***#
$t_{1/2z}$	h	1.12 ± 0.36	2.11 ± 1.10	4.44 ± 1.84	6.88 ± 3.53***#
T_{max}	h	0.50 ± 0.00	0.79 ± 0.64	0.46 ± 0.10	0.46 ± 0.10
CL _{z/F}	L·h ⁻¹ ·kg ⁻¹	145.5 ± 30.86	80.96 ± 13.72***	37.32 ± 6.41***##	23.30 ± 4.78***##
C _{max}	μg/L	282.17 ± 76.26	340.83 ± 101.79	416.00 ± 148.02	548.33 ± 91.85*
Increased AUC ^a		100.00%	183.73%	326.58%	435.04%

Notes: Formulation 1 composed Cap 90-EL35-PEG (CEP) and formulation 2 composed Cap 90-EL35-THP (CET) for delivery of both TGP and nobiletin (N). * $P < 0.05$, ** $P < 0.01$, *** $P < 0.001$ indicate significant differences from free TGP group; # $P < 0.05$, ## $P < 0.01$, ### $P < 0.001$ indicate significant differences from TGP+N treatment group. ^a increased AUC was calculated by dividing the AUC of testing group to AUC (TGP).

Moreover, an increased intracellular accumulation of TGP was achieved after treatment with the CEP and CET formulations in THP-1-P gp cells, namely, 2.53 ± 0.05 - and 3.56 ± 0.15 -fold higher than that of TGP alone. Moreover, we found that, given the same dosage of TGP, the intracellular TGP content of the CET formulation in THP-1-P-gp cells was even higher than that of sensitive THP-1 cells, indicating that it not only suppressed efflux but also enhanced transport into lymphocytes. Consequently, the CET formulation dramatically inhibited cytokines in both resistant THP-1-P-gp cells and sensitive THP-1 cells.

Altogether, the developed TGP-N-loaded SNEDD formulation remarkably increased the intracellular drug concentrations in drug-resistant THP-1-P gp cells and sensitive THP-1 cells, which led to enhanced anti-inflammatory effects.

Refractory RA animal model

In the preliminary study, we compared the expression of P-gp on lymphocytes isolated from three commonly used RA animal models in mice or rats (as illustrated in Supplementary Fig. 4). Interestingly, only AIA rats induced by intradermal injection into the left hind paw had significantly increased P-gp levels in their lymphocytes. Our data demonstrated that there was a remarkable increase (6.65-fold) in the proportion of P-gp-expressing lymphocytes ($11.97\% \pm 3.57\%$, $P < 0.001$) in this AIA rat model compared with that of normal rats ($1.80\% \pm 0.65\%$) (Fig. 5a). This finding was consistent with the markedly increased expression of P-gp in lymphocytes isolated from AIA rats in comparison with normal rats. (Fig. 7a).

Next, we wanted to confirm whether the overexpression of P-gp in the lymphocytes of AIA rats caused drug resistance, similar to the phenomenon observed in patients with refractory RA. In lymphocytes isolated from AIA rats, MTX (10 μM) and TGP (10 μM) could not suppress the expression of inflammatory cytokines, including TNF-α, IL-1β, and IL-6, induced by LPS, as shown in Fig. 5b. However, at the same dosage, MTX and TGP showed notable anti-inflammatory effects in normal rat peritoneal lymphocytes. These results confirmed that the overexpression of P-gp in lymphocytes isolated from AIA rats led to resistance to MTX and TGP.

Moreover, we evaluated whether the P-gp inhibitor and CET formulation could overcome the drug resistance induced by P-gp in lymphocytes isolated from AIA rats. After administration of the CET formulation, our data showed an obvious reduction in the percentages of P-gp-expressing lymphocytes in the AIA rats ($3.26\% \pm 0.83\%$, $P < 0.001$) compared with that in the TGP group ($9.17\% \pm 2.64\%$) or model group. Treatment with the P-gp inhibitor N with TGP showed a mild reduction in the proportion of P-gp-expressing lymphocytes in the AIA rats ($5.77\% \pm 0.47\%$) (Fig. 5a). Consistent with the inhibitory effect on the proportion of

P-gp-expressing lymphocytes in the AIA rats, we found that the cotreatment with N enhanced the anti-inflammatory effects of TGP ($P < 0.05$); however, the CET formulation significantly inhibited the expression of cytokines and successfully overcame resistance to TGP ($P < 0.01$) (Fig. 5c).

To further confirm the “refractory” characteristics of our RA animal model, we evaluated the anti-arthritis effects of MTX at a dosage of 0.5 mg/kg every 3 days, which has been shown to have notable anti-arthritis effects in the literature [33–35]. However, at this dosage, MTX did not exhibit obvious treatment efficacy in our AIA rat model. In fact, a high dosage treatment of MTX (7.6 mg/kg per week) showed a marked efficacy in controlling the symptoms of arthritis in the AIA rats (Fig. 6) with a significantly reduced arthritis score (2.33 ± 2.16 , $P < 0.001$). Interestingly, the AIA rats given a low dosage of MTX treatment ($8.48\% \pm 1.48\%$) had a relatively high percentage of P-gp-expressing lymphocytes in comparison with the rats treated with the high dosage of MTX ($2.27\% \pm 0.85\%$, $P < 0.001$).

All these data indicated that our AIA rat model showed partial resistance to MTX and TGP, which was due to the high expression of P-gp in lymphocytes, as observed in clinically refractory RA.

CET enhanced the anti-arthritis effects in the AIA rats

Here, we compared the anti-arthritis effects of the developed SNEDDS formulation (CET) with TGP alone and in combination with N (TGP + N). As shown in Fig. 6a and b, the arthritis score (11.67 ± 0.52 , $P < 0.001$) and edema of the right hind paw of the AIA rats increased sharply after the 9th day of injection compared with those of normal rats, which was consistent with the significant swelling in the morphology observations (Fig. 6c).

When treated alone, TGP exerted no obvious anti-arthritis effects in the AIA rats, which was similar to the effect of MTX at a dosage of 0.5 mg/kg every 3 days. After 27 days of treatment, CET formulation attenuated the swelling and arthritis scores (5.50 ± 2.26 , $P < 0.001$) of AIA rats, which was stronger than the effects of TGP and N cotreatment (8.67 ± 2.80 , $P < 0.05$) (Fig. 6b). Furthermore, CET treatment showed notable anti-inflammatory effects by reducing serum cytokines such as IL-1, TNF-α, and IL-6 ($P < 0.01$ or $P < 0.001$) (Fig. 6f).

Compared with normal rats, vehicle-treated AIA rats exhibited rough bone surfaces, joint space narrowing, and severe bone erosion based on the three-dimensional micro-CT imaging data of the joints of AIA rats (Fig. 6d). Both the CET formulation and high dosage of MTX treatment showed a marked protective effect on the joints and ameliorated bone erosion. Moreover, histological results demonstrated that CET treatment suppressed the infiltration of immune cells and inflammation within joints (Fig. 6e).

All these results indicated that the TGP-N coloaded CET formulation is a promising therapeutic strategy for the treatment

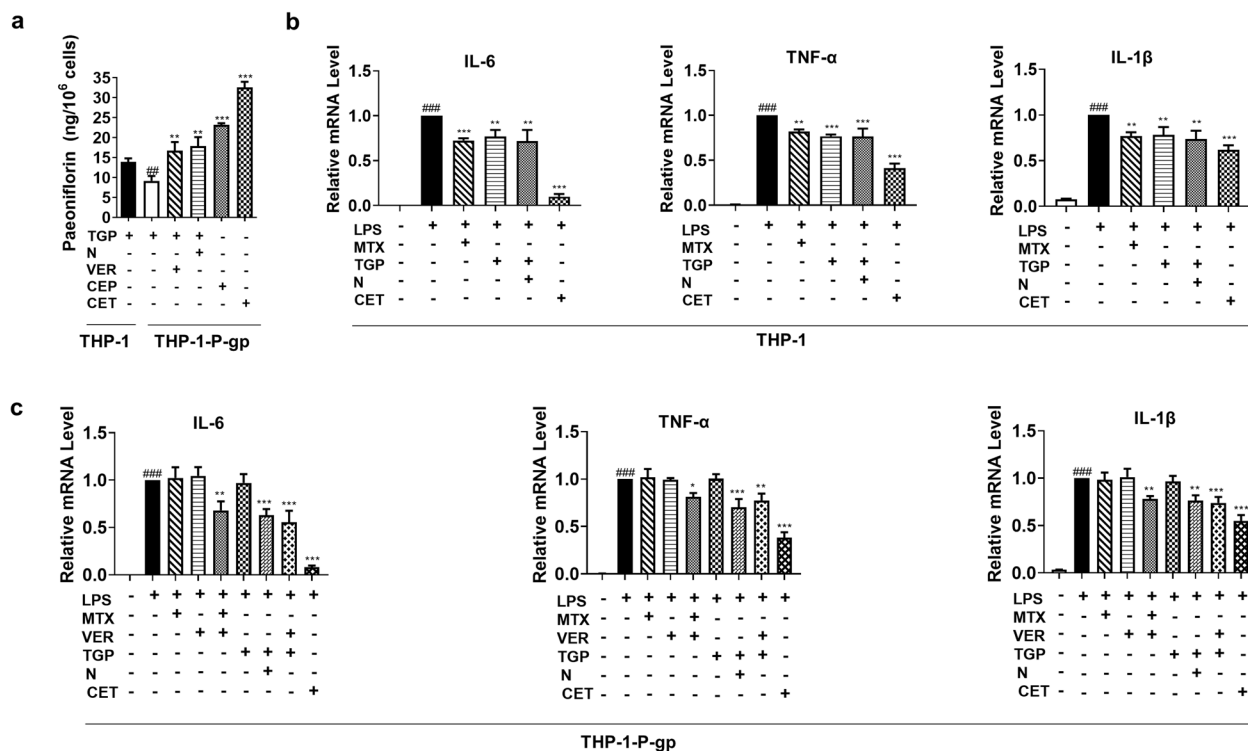


Fig. 4 Total glucosides of paeony (TGP) and nobiletin (N) codelivered in the SNEDDS formulations overcome resistance in P-gp-overexpressing THP cells. **a** In comparison with THP-1 cells, THP-1-P-gp cells exhibited increased intracellular concentrations of TGP (evaluated as paeoniflorin) by SNEDD formulation (CET) or P-gp inhibitor N and verapamil (VER). $^{##}P < 0.01$, vs. THP-1 cells. $^{**}P < 0.01$, $^{***}P < 0.001$ vs. TGP treatment group. THP-1-P-gp cells showed resistance to MTX and TGP (**c**) at the same dosage, which reduced the mRNA expression levels of IL-6, TNF- α , and IL-1 β in the THP-1 cells (**b**), while the CET formulation overcame the resistance and increased therapeutic effects. The dosage of TGP (paeoniflorin 10 μ M), verapamil (VER 2 μ M), methotrexate (MTX 2.5 μ M), and nobiletin (N 2 μ M) in THP-1 and THP-1-P-gp cells. Data expressed as the mean \pm SD. $^{*}P < 0.05$, $^{**}P < 0.01$, $^{***}P < 0.001$ vs. LPS-stimulated cells, $^{###}P < 0.001$, vs. normal cells.

of refractory RA because of the boosted anti-arthritis effects in preventing inflammation and bone destruction in AIA rats, which are resistant to TGP and MTX.

Mechanisms for regulating P-gp by CET formulation

To explore the underlying mechanisms of CET formulations, the protein expression of P-gp and the intracellular contents of paeoniflorin were determined in lymphocytes isolated from AIA rats. Consistent with the percentages of P-gp-expressing lymphocytes observed by flow cytometry, we found that the protein expression of P-gp was significantly higher in lymphocytes isolated from the AIA rats (1.61 \pm 0.31-fold, $P < 0.05$) than in lymphocytes from normal rats, as shown in Fig. 7a.

The expression of P-gp is transcriptionally regulated by hypoxia-inducible factor-1 α (HIF-1 α) in tumors [44], while the inhibition of HIF-1 α reverses drug resistance in colon cancer by downregulating P-gp [45]. Moreover, HIF- α plays a key role in controlling immune cell metabolism and functions [46]. We noticed a marked increase in the levels of HIF-1 α (3.45 \pm 0.24-fold, $P < 0.001$) in the AIA rat lymphocytes compared with lymphocytes from normal rats. Lymphocytes from CET-treated AIA rats exhibited significantly reduced expression of HIF-1 α and P-gp ($P < 0.001$), which was similar to the TGP + N cotreatment group ($P < 0.001$).

Moreover, the activated PI3K/Akt pathway plays a key role in inducing drug resistance during cancer and modulates the expression and function of P-gp [47]. Here, we also observed abnormal activation of the PI3K/Akt pathway, as indicated by the increased phosphorylated AKT in the lymphocytes of AIA rats, which may also contribute to the overexpression of P-gp in AIA rats (Fig. 7). Treatment with CET or cotreatment with TGP + N inhibited AKT phosphorylation in lymphocytes from the AIA rats ($P < 0.001$).

Notably, the intracellular concentrations of paeoniflorin in lymphocytes isolated from CET-treated AIA rats or cotreated TGP + N rats were 3.20 \pm 0.23-fold ($P < 0.001$) and 1.94 \pm 0.28-fold ($P < 0.01$, Fig. 7e) higher than those of the TGP group.

All these data indicated that the CET formulation and cotreatment with N overcame the drug resistance induced by P-gp via downregulation of the PI3K/AKT and HIF-1 α pathways in the AIA rat lymphocytes, leading to enhanced intracellular drug concentrations and anti-arthritis effects.

DISCUSSION

Recent clinical studies showed that P-gp was overexpressed by lymphocytes [9] and fibroblast-like synoviocytes [7] from patients with refractory RA and/or high disease activity, which is the potential reason for drug resistance to corticosteroids and DMARDs [48]. Moreover, P-gp-mediated efflux also contributed to the low bioavailability of drugs such as TGP, leading to the limited therapeutic response in a subset of RA patients after treatment with TGP. Therefore, the inhibition and/or reduction of P-gp provides a therapeutic approach that not only overcomes drug resistance [8] but also enhances the therapeutic effect of TGP in the treatment of refractory RA patients.

In this study, the P-gp inhibitor nobiletin [18] was used in combination with TGP and codelivered in the developed novel SNEDDS formulations. Compared with conventional methods for the development of a SNEDDS [49], the method employed in this study for screening SNEDDS excipients was helpful in understanding the emulsification efficiency of different surfactants for the selected oily phase used for oral drug delivery. Moreover, the drug loading ability for N in a SNEDDS developed by Yao et al. was

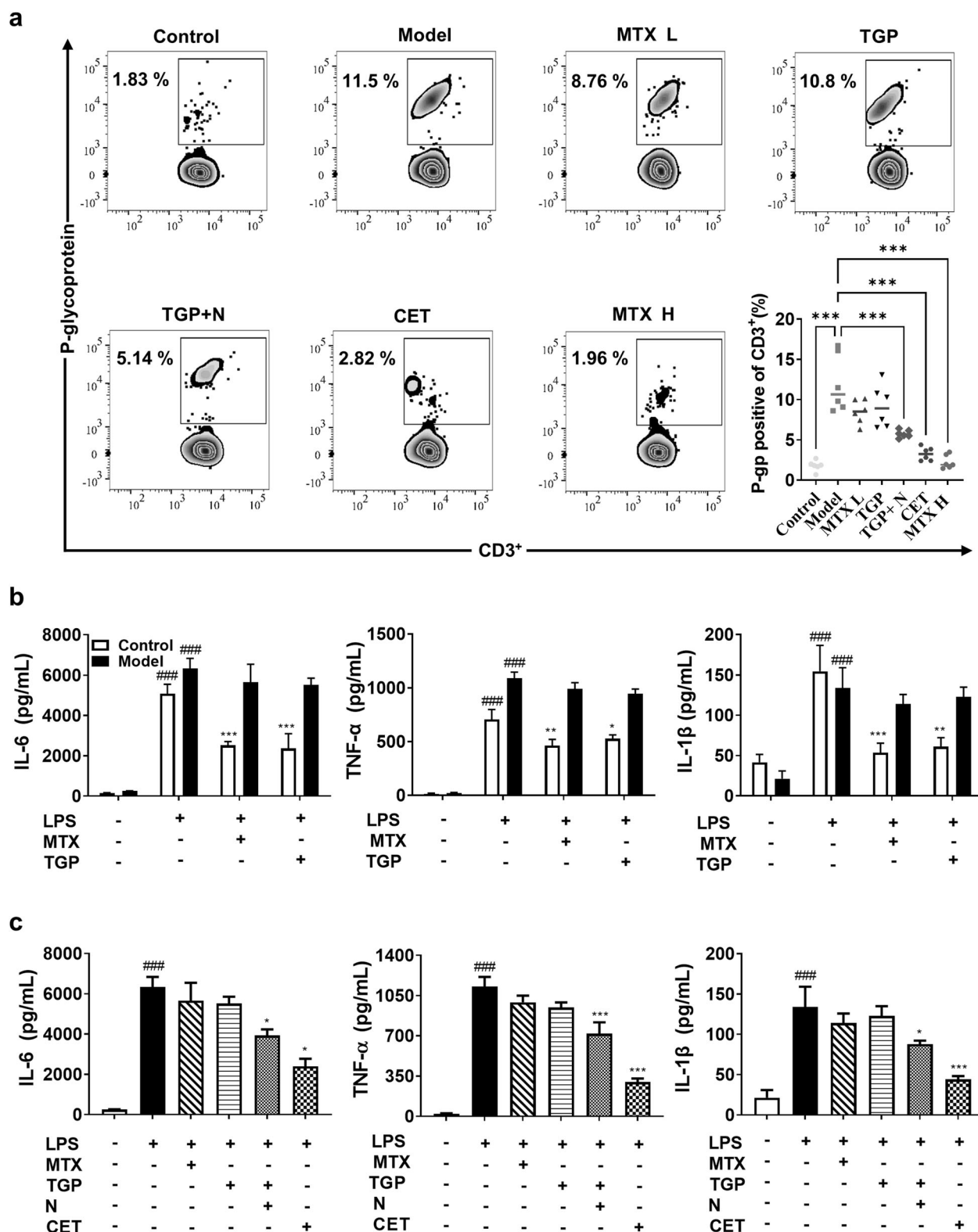


Fig. 5 P-gp-overexpressing lymphocytes from the AIA rats led to resistance to MTX and TGP. **a** Percentage of P-glycoprotein (P-gp)-overexpressing peripheral lymphocytes in AIA rats was compared with that in normal rats and drug-treated rats, as determined by flow cytometry ($n = 6$). **b** Lymphocytes isolated from the AIA rats exhibited drug resistance to MTX and TGP, as indexed by the levels of inflammatory cytokines, including IL-1 β , IL-6 and TNF- α , induced by 1 μ g/mL LPS. At the same dosage, TGP and MTX decreased these cytokines in normal rat lymphocytes. **c** CET significantly suppressed the production of IL-6, TNF- α , and IL-1 β induced by LPS, which was consistent with its effect on inhibiting P-gp. The dosage of TGP (calculated based on 10 μ M paeoniflorin), methotrexate (MTX 10 μ M), and nobiletin (N 2 μ M). All data are presented as the mean \pm SD. * $P < 0.01$, ** $P < 0.01$, *** $P < 0.001$ vs. LPS-stimulated cells, ### $P < 0.001$, vs. unstimulated cells.

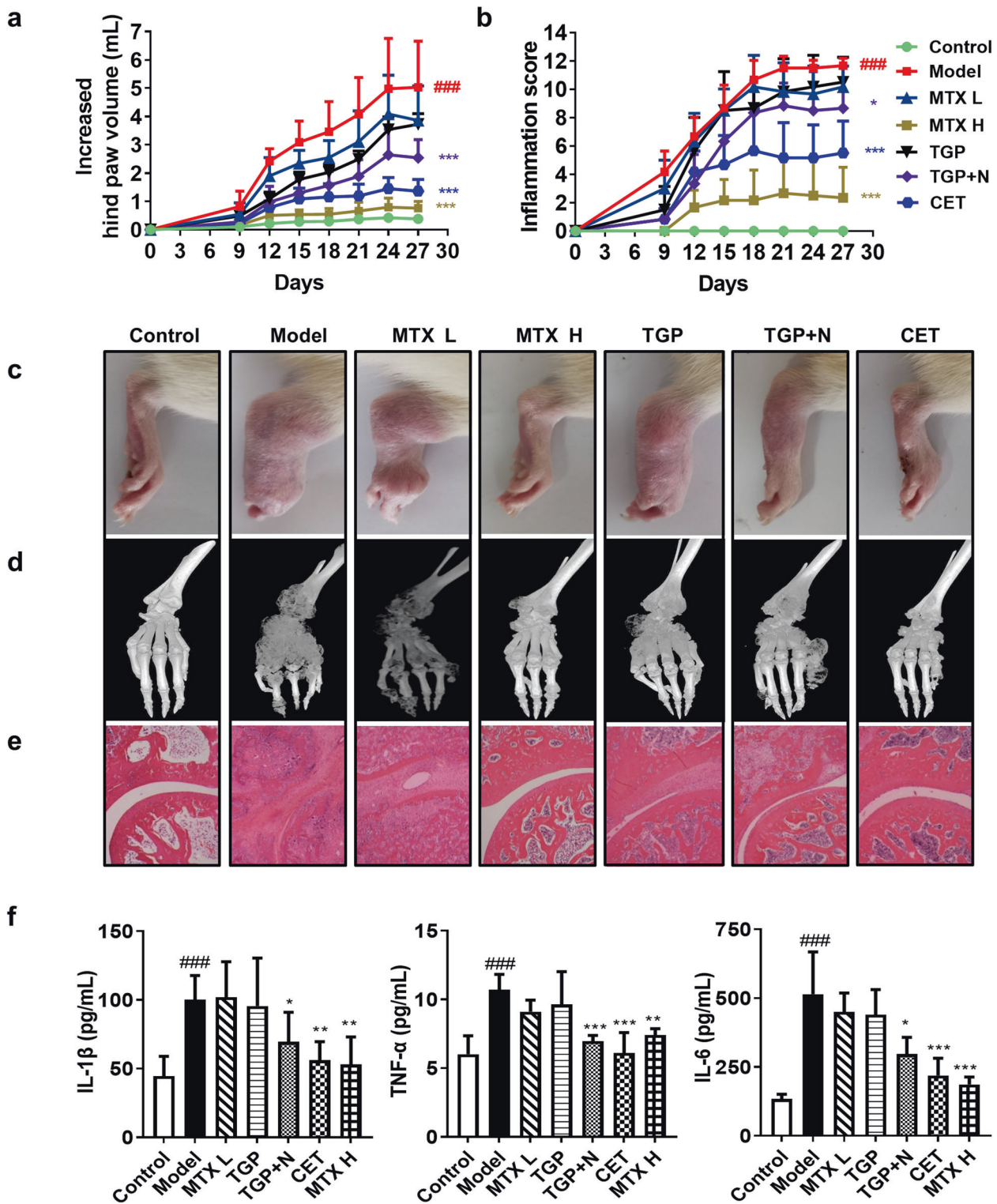


Fig. 6 Anti-arthritis effects of the SNEDDS formulation on a rat adjuvant-induced arthritis (AIA) model ($n = 6$). **a** Edema of the right hind paw, **(b)** arthritic scores, and representative histological images of the right hind paw with **(c)** photographs of joint swelling, **(d)** micro-CT, and **(e)** hematoxylin and eosin (H&E) staining of the AIA rats. **f** Inhibiting effects of the CET formulation on serum inflammatory cytokines. All data were presented as the mean \pm SD. * $P < 0.05$, ** $P < 0.01$, *** $P < 0.001$ vs. the model group; #### $P < 0.001$ vs. the control group.

15 mg/g [50], but we could load 30 mg/g of N in the CET-SNEDDS formulation, representing that the suitable surfactant/or cosurfactant used here resulted in a high emulsification efficiency.

Nanoparticles engineered for systemic administration into the body have great potential for the treatment of complex human

diseases. However, despite significant efforts to improve their treatment efficacy, significant quantities of nanoparticles in circulation were eventually cleared by macrophages of the mononuclear phagocytic system [51]. Nanoparticles smaller than 100 nm were endocytosed by macrophages [52]. However, if the

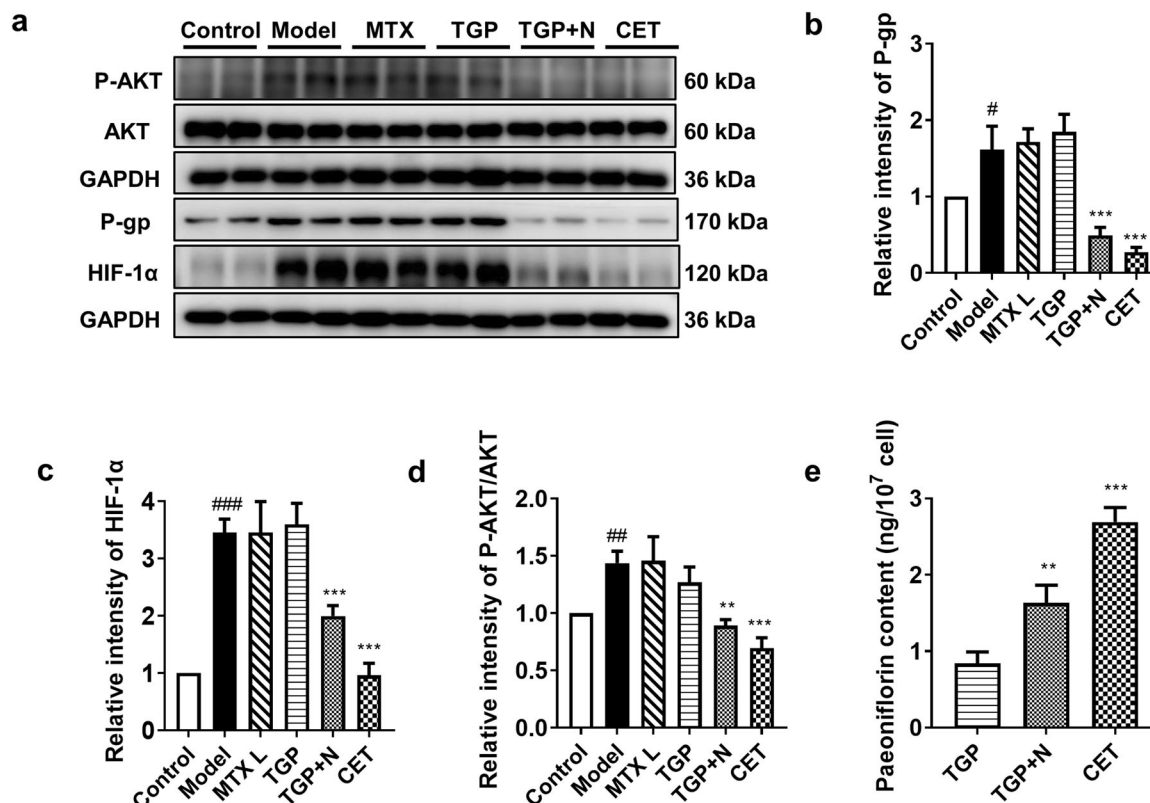


Fig. 7 CET reduced the overexpression of P-gp by modulating the PI3K/AKT and HIF1- α pathways in lymphocytes from the AIA rats. **a** Protein expression of P-gp, phosphorylated AKT, total AKT, and HIF1- α in lymphocytes isolated from the rats, as evaluated by immunoblotting. The relative protein expression levels of P-gp (**b**), HIF1- α (**c**) and phosphorylated AKT/total AKT (**d**) were examined ($n = 6$). **e** Moreover, CET or the cotreatment of TGP with nobiletin (N) significantly increased the intracellular content of paeoniflorin in the AIA rat lymphocytes compared with TGP-treated rats. All data were presented as the mean \pm SD. $**P < 0.01$, $***P < 0.001$ vs. model group; $\#P < 0.05$, $##P < 0.01$, $###P < 0.001$, vs. the control group.

nanoparticle size was below 20 nm, endocytosis hardly occurred because the adhesion energy was too low to compensate for the bending energy [53, 54]. Here, the particle size of CET was less than 20 nm; therefore, CET was not expected to be recognized by the mononuclear phagocytic system.

The absolute bioavailability of paeoniflorin was approximately 3% after TGP was given due to poor absorption and P-gp-mediated efflux [15, 16]. After 4 hours of the oral administration of TGP, we noticed that the plasma concentration of paeoniflorin dropped rapidly and fell below the detection limit. Therefore, the in vivo drug concentrations were quickly below the minimum effective concentration, which may be the main reasons that led to the slow onset of action and limited response in RA patients after the oral administration of TGP [14, 15]. CET formulation significantly increased the plasma concentrations and bioavailability of TGP after a single dose. In THP-1-P-gp cells, Caco-2 cells, and an ex vivo intestinal perfusion model, our results demonstrated that nobiletin significantly inhibited the efflux mediated by P-gp, while SNEDD formulations further enhanced the permeability and absorption of TGP, both of which corroborated the improved bioavailability of TGP. Moreover, paeoniflorin in TGP has relatively high levels in immune-relevant tissues such as the spleen, thymus, and bone [55], suggesting a potential for immunoregulatory activities.

To the best of our knowledge, we are the first to develop a rat model of RA to mimic the features of human refractory RA, which contained overexpressed P-gp in lymphocytes and was resistant to treatment. This finding is consistent with clinical evidence that P-gp is overexpressed in lymphocytes from patients with refractory RA or high disease activity [8, 9].

The overexpression of P-gp in lymphocytes from the AIA rats was positively related to the severity of arthritis in rats. Most importantly, these lymphocytes from AIA rats showed resistance to treatment with MTX or TGP. However, at the same dosage, MTX or TGP had remarkable anti-inflammatory effects on the lymphocytes of normal rats.

We also noticed that effective treatments with a high dosage of MTX ($2.27\% \pm 0.85\%$, $P < 0.001$) resulted in a relatively low percentage of P-gp-overexpressing lymphocytes in comparison with the rats treated with a low dosage of MTX ($8.48\% \pm 1.48\%$). High expression of P-gp in lymphocytes was observed in patients with highly active RA and was positively correlated with disease activity [7, 8]. Many cytokines, such as interleukin 2 and tumor necrosis factor- α , increase P-gp expression and activity [56], which may be the reason for the positive correlation between the high expression of P-gp and the disease activity of RA. Therefore, we observed high P-gp expression in AIA rats with high arthritis scores, such as the vehicle-treated group or the low-dosage MTX group. In contrast, high-dosage MTX treatment effectively suppressed inflammation and the immune response at the beginning of arthritis induction, which resulted in a limited increase in P-gp expression. Therefore, we observed a low percentage of P-gp-overexpressing lymphocytes in rats treated with a high dosage of MTX. Our study indicated that the expression of P-gp was a potential marker for disease progression and drug resistance in RA.

To understand the mechanisms of increased P-gp levels in the AIA rat lymphocytes and the anti-arthritis effect of CET, we evaluated the expression of PI3K/AKT and HIF1- α pathways, as both of them have been shown to regulate the expression of P-gp

in cancer [44, 47]. Cotreatment with TGP and N and the CET formulation successfully reduced the expression of HIF-1 and phosphorylation of AKT in the AIA lymphocytes, which was consistent with the reduction in P-gp expression. Our data indicated that the PI3K/AKT and HIF1- α pathways may be upstream factors for the overexpression of P-gp in the AIA rat lymphocytes. Moreover, it is well known that HIF1- α plays a key role in the function and metabolism of immune cells [46], while the PI3K/Akt/mTOR pathway deregulates the proliferation and aberrant survival of immune cells [57]. Therefore, the suppression of these pathways may also be involved in the therapeutic effects of the CET formulation.

CONCLUSION

To summarize, the codelivery of the P-gp inhibitor nobiletin and TGP with the optimized SNEDDS composed of capryol 90, cremophor EL35, and transcutool H (CET) successfully improved the bioavailability of TGP and overcame drug resistance mediated by P-gp overexpression. The enhanced therapeutic efficacy of CET in the refractory RA animal model was due to the increased concentrations of target drugs in the lymphocytes of AIA rats by reducing the expression of P-gp and suppressing the AKT/HIF-1 α pathways. These inspiring outcomes suggest that cotreatment with a P-gp inhibitor in the SNEDDS formulation has great potential to overcome resistance to other antirheumatoid drugs, such as corticosteroids and MTX, thereby representing a promising treatment strategy for refractory RA.

ACKNOWLEDGEMENTS

This work was financially supported by the Science and Technology Development Fund, Macao SAR, China (File no. 0067/2019/A2 and 0075/2019/AMJ).

AUTHOR CONTRIBUTIONS

YX and HZ contributed equally and designed the experiments; BQ, DCZ, and CTM developed the concept and discussed experiments; BQ developed the nano-SNEDDS formulation and carried out the PK study; BQ, DCZ, and CTM modified the arthritis animal model, isolated lymphocytes, carried out all the flow cytometry experiments and results analysis, and wrote the original manuscript. XLW and ZQL provided ideas for the nanoformulation and technical assistance. YX supervised all research phases and revised the paper.

ADDITIONAL INFORMATION

Supplementary information The online version contains supplementary material available at <https://doi.org/10.1038/s41401-021-00801-6>.

Competing interests: The authors declare no competing interests.

REFERENCES

- Chen Z, Li XP, Li ZJ, Xu L, Li XM. Reduced hepatotoxicity by total glucosides of paeony in combination treatment with leflunomide and methotrexate for patients with active rheumatoid arthritis. *Int Immunopharmacol*. 2013;15:474–7.
- Smolen JS, Aletaha D, McInnes IB. Rheumatoid arthritis. *Lancet*. 2016;388:2023–38.
- Cojocaru M, Cojocaru IM, Silosi I, Vrabie CD, Tanasescu R. Extra-articular manifestations in rheumatoid arthritis. *Maedica*. 2010;5:286–91.
- Burmester GR. RA in 2011: Advances in diagnosis, treatment and definition of remission. *Nat Rev Rheumatol*. 2012;8:65–6.
- Saag KG, Teng GG, Patkar NM, Anuntiyo J, Finney C, Curtis JR, et al. American College of Rheumatology 2008 recommendations for the use of nonbiologic and biologic disease-modifying antirheumatic drugs in rheumatoid arthritis. *Arthritis Rheum*. 2008;59:762–84.
- Buch MH, Eyre S, McGonagle D. Persistent inflammatory and non-inflammatory mechanisms in refractory rheumatoid arthritis. *Nat Rev Rheumatol*. 2021;17:17–33.
- Liu YM, Chen JW, Chen LX, Xie X, Mao N. Overexpression of P-glycoprotein on fibroblast-like synoviocytes in refractory rheumatoid arthritis patients: a potential mechanism for multidrug resistance in rheumatoid arthritis treatment. *Genet Mol Res*. 2016;15. <https://doi.org/10.4238/gmr.15027927>.
- Tsujimura S, Saito K, Nawata M, Nakayama S, Tanaka Y. Overcoming drug resistance induced by P-glycoprotein on lymphocytes in patients with refractory rheumatoid arthritis. *Ann Rheum Dis*. 2008;67:380–8.
- Tsujimura S, Tanaka Y. Disease control by regulation of P-glycoprotein on lymphocytes in patients with rheumatoid arthritis. *World J Exp Med*. 2015;5:225–31.
- Yu J, Xiao Z, Zhao R, Lu C, Zhang Y. Paeoniflorin suppressed IL-22 via p38 MAPK pathway and exerts anti-psoriatic effect. *Life Sci*. 2017;180:17–22.
- Zhou Y, Jin L, Kong F, Zhang H, Fang X, Chen Z, et al. Clinical and immunological consequences of total glucosides of paeony treatment in Sjogren's syndrome: a randomized controlled pilot trial. *Int Immunopharmacol*. 2016;39:314–9.
- Wei CC, You FT, Mei LY, Jian S, Qiang CY. Total glucosides of paeony prevents juxta-articular bone loss in experimental arthritis. *BMC Complement Alter Med*. 2013;13:186.
- Zou ZM, Xu LZ, Yang SL. HPLC fingerprinting of total glucosides of paeony. *Acta Pharm Sin*. 2003;38:46–9.
- Wang C, Wei W. Research progress of pharmacokinetic study on paeoniflorin. *Chin Pharm Bull*. 2014;30:1646–50.
- Liu ZQ, Zhou H, Liu L, Jiang ZH, Wong YF, Xie Y, et al. Influence of co-administered sinomenine on pharmacokinetic fate of paeoniflorin in unrestrained conscious rats. *J Ethnopharmacol*. 2005;99:61–7.
- Liu ZQ, Jiang ZH, Liu L, Hu M. Mechanisms responsible for poor oral bioavailability of paeoniflorin: Role of intestinal disposition and interactions with sinomenine. *Pharmacol Res*. 2006;23:2768–80.
- Huang H, Li L, Shi W, Liu H, Yang J, Yuan X, et al. The multifunctional effects of nobiletin and its metabolites in vivo and in vitro. *Evid Based Complement Altern Med*. 2016;2016:2918796.
- Ma W, Feng S, Yao X, Yuan Z, Liu L, Xie Y. Nobiletin enhances the efficacy of chemotherapeutic agents in ABCB1 overexpression cancer cells. *Sci Rep*. 2015;5:18789.
- Feng SL, Tian Y, Huo S, Qu B, Liu RM, Xu P, et al. Nobiletin potentiates paclitaxel anticancer efficacy in A549/T xenograft model: Pharmacokinetic and pharmacological study. *Phytomedicine*. 2020;67:153141.
- Baheti A, Srivastava S, Sahoo D, Lowalekar R, Panda BP, Padhi BK, et al. Development and pharmacokinetic evaluation of industrially viable self-microemulsifying drug delivery systems (SMEDDS) for terbinafine. *Curr Drug Deliv*. 2015. Online ahead of print.
- Park K. The lack of IVVC for monoacyl phospholipid-based self-emulsifying drug delivery systems. *J Control Release*. 2017;255:279.
- Kim DW, Kwon MS, Yousaf AM, Balakrishnan P, Park JH, Kim DS, et al. Comparison of a solid SMEDDS and solid dispersion for enhanced stability and bioavailability of clopidogrel napadisilate. *Carbohydr Polym*. 2014;114:365–74.
- Friedl H, Dunnhaupt S, Hintzen F, Waldner C, Parikh S, Pearson JP, et al. Development and evaluation of a novel mucus diffusion test system approved by self-nanoemulsifying drug delivery systems. *J Pharm Sci*. 2013;102:4406–13.
- Rohrer J, Partenhauser A, Hauptstein S, Gallati CM, Matuszczak B, Abdulkarim M, et al. Mucus permeating thiolated self-emulsifying drug delivery systems. *Eur J Pharm Biopharm*. 2016;98:90–7.
- Zupancic O, Partenhauser A, Lam HT, Rohrer J, Bernkop-Schnurch A. Development and in vitro characterisation of an oral self-emulsifying delivery system for daptomycin. *Eur J Pharm Sci*. 2016;81:129–36.
- Suchaon W, Pereira de Sousa I, Netsomboon K, Lam HT, Laffleur F, Bernkop-Schnurch A. Development and in vitro evaluation of zeta potential changing self-emulsifying drug delivery systems for enhanced mucus permeation. *Int J Pharm*. 2016;510:255–62.
- Jain S, Jain AK, Pohekar M, Thanki K. Novel self-emulsifying formulation of quercetin for improved in vivo antioxidant potential: implications for drug-induced cardiotoxicity and nephrotoxicity. *Free Radic Biol Med*. 2013;65:117–30.
- Dhumal DM, Kothari PR, Kalhapure RS, Akamanchi KG. Self-microemulsifying drug delivery system of curcumin with enhanced solubility and bioavailability using a new semi-synthetic bicephalous heterolipid: in vitro and in vivo evaluation. *RSC Adv*. 2015;5:90295–306.
- Yin YM, Cui FD, Mu CF, Choi MK, Kim JS, Chung SJ, et al. Docetaxel microemulsion for enhanced oral bioavailability: preparation and in vitro and in vivo evaluation. *J Control Release*. 2009;140:86–94.
- Chen J, Lin H, Hu M. Metabolism of flavonoids via enteric recycling: role of intestinal disposition. *J Pharmacol Exp Ther*. 2003;304:1228–35.
- Jia X, Chen J, Lin H, Hu M. Disposition of flavonoids via enteric recycling: enzyme-transporter coupling affects metabolism of biochanin A and formononetin and excretion of their phase II conjugates. *J Pharmacol Exp Ther*. 2004;310:1103–13.
- Yuan ZW, Li YZ, Liu ZQ, Feng SL, Zhou H, Liu CX, et al. Role of tangeretin as a potential bioavailability enhancer for silybin: Pharmacokinetic and pharmacological studies. *Pharmacol Res*. 2018;128:153–66.
- Tang H, Wu YJ, Xiao F, Wang B, Asenso J, Wang Y, et al. Regulation of CP-25 on P-glycoprotein in synoviocytes of rats with adjuvant arthritis. *Biomed Pharmacother*. 2019;119:109432.

34. Asenso J, Yu J, Xiao F, Zhao M, Wang J, Wu Y, et al. Methotrexate improves the anti-arthritis effects of Paeoniflorin-6'-O-benzene sulfonate by enhancing its pharmacokinetic properties in adjuvant-induced arthritis rats. *Biomed Pharmacother.* 2019;112:108644.
35. Yang X, Zhao Y, Jia X, Wang C, Wu Y, Zhang L, et al. CP-25 combined with MTX/LEF ameliorates the progression of adjuvant-induced arthritis by the inhibition on GRK2 translocation. *Biomed Pharmacother.* 2019;110:834–43.
36. Chang Y, Wu Y, Wang D, Wei W, Qin Q, Xie G, et al. Therapeutic effects of TACI-Ig on rats with adjuvant-induced arthritis via attenuating inflammatory responses. *Rheumatology (Oxf).* 2011;50:862–70.
37. Zhou J, Wang LP, Feng X, Fan DD, Zang WJ, Wang B. Synthetic peptides from heat-shock protein 65 inhibit proinflammatory cytokine secretion by peripheral blood mononuclear cells from rheumatoid arthritis patients. *Clin Exp Pharmacol Physiol.* 2014;41:67–72.
38. Zhang P, Liu Y, Feng N, Xu J. Preparation and evaluation of self-microemulsifying drug delivery system of oridonin. *Int J Pharm.* 2008;355:269–76.
39. Liu D, Tian Y, Zhang ZH, Jia XB. Preparation of self-microemulsifying drug delivery system and similarity analysis on dissolution behavior of ginkgolides components. *Zhong Cao Yao.* 2016;47:3798–804.
40. Chen X, Fu ZJ. Formulation optimization of self-microemulsion loaded with total alkaloid from *Nelumbinis Plumula* by central composite design-response surface method. *Chin Tradit Pat Med* 2016;38:1490–5.
41. Ke Z, Hou X, Jia XB. Design and optimization of self-nanoemulsifying drug delivery systems for improved bioavailability of cycloviobuxine D. *Drug Des Devel Ther.* 2016;10:2049–60.
42. Giacomini KM, Huang SM, Tweedie DJ, Benet LZ, Brouwer KL, Chu X, et al. Membrane transporters in drug development. *Nat Rev Drug Discov.* 2010;9:215–36.
43. Hu PY, Liu D, Zheng Q, Wu Q, Tang Y, Yang M. Elucidation of transport mechanism of paeoniflorin and the influence of ligustilide, senkyunolide I and senkyunolide A on paeoniflorin transport through Mdr1-Mdr3 cells as blood-brain barrier in vitro model. *Molecules* 2016;21:300.
44. Wartenberg M, Ling FC, Müschen M, Klein F, Acker H, Gassmann M, et al. Regulation of the multidrug resistance transporter P-glycoprotein in multicellular tumor spheroids by hypoxia-inducible factor (HIF-1) and reactive oxygen species. *Faseb J.* 2003;17:503–5.
45. Chen J, Ding Z, Peng Y, Pan F, Li J, Zou L, et al. HIF-1 α inhibition reverses multidrug resistance in colon cancer cells via downregulation of MDR1/P-glycoprotein. *PLoS One.* 2014;9:e98882.
46. Meng X, Grötsch B, Luo Y, Knaup KX, Wiesener MS, Chen XX, et al. Hypoxia-inducible factor-1 α is a critical transcription factor for IL-10-producing B cells in autoimmune disease. *Nat Commun.* 2018;9:251.
47. Liu R, Chen Y, Liu G, Li C, Song Y, Cao Z, et al. PI3K/AKT pathway as a key link modulates the multidrug resistance of cancers. *Cell Death Dis.* 2020;11:797.
48. Picchianti-Diamanti A, Rosado MM, Scarsella M, Lagana B, D'Amelio R. P-glycoprotein and drug resistance in systemic autoimmune diseases. *Int J Mol Sci.* 2014;15:4965–76.
49. Date AA, Nagarsenker MS. Design and evaluation of self-nanoemulsifying drug delivery systems (SNEDDS) for cefpodoxime proxetil. *Int J Pharm.* 2007;329:166–72.
50. Yao J, Lu Y, Zhou JP, Ping QN. Preparation of nobiletin-loaded self-microemulsifying system and its absorption kinetics in rat intestines. *J Chin Pharm Univ.* 2007;38:35–8.
51. Oh N, Park JH. Surface chemistry of gold nanoparticles mediates their exocytosis in macrophages. *ACS Nano.* 2014;8:6232–41.
52. Lunov O, Syrovets T, Loos C, Beil J, Delacher M, Tron K, et al. Differential uptake of functionalized polystyrene nanoparticles by human macrophages and a monocytic cell line. *ACS Nano.* 2011;5:1657–69.
53. Zhang S, Li J, Lykotrafitis G, Bao G, Suresh S. Size-dependent endocytosis of nanoparticles. *Adv Mater.* 2009;21:419–24.
54. Chithrani BD, Chan WC. Elucidating the mechanism of cellular uptake and removal of protein-coated gold nanoparticles of different sizes and shapes. *Nano Lett.* 2007;7:1542–50.
55. Fei F, Yang H, Peng Y, Wang P, Wang S, Zhao Y, et al. Sensitive analysis and pharmacokinetic study of the isomers paeoniflorin and albiflorin after oral administration of Total Glucosides Of White Paeony Capsule in rats. *J Chromatogr B Anal Technol Biomed Life Sci.* 2016;1022:30–7.
56. Fernandez C, Buysse M, GermanFattal M, Gimenez F. Influence of the pro-inflammatory cytokines on P-glycoprotein expression and functionality. *J Pharm Pharm Sci.* 2004;7:359–71.
57. Malemud CJ. The PI3K/Akt/PTEN/mTOR pathway: a fruitful target for inducing cell death in rheumatoid arthritis? *Future Med Chem.* 2015;7:1137–47.